ELSEVIER

Thermochimica Acta 249 (1995) 269–283

thermochimica acta

Modifications to the binary phase diagram of the alkane mixtures n-C_{23}–n-C_{24}

A. Sabour, J.B. Bourdet, M. Bouroukba, M. Dirand *

Laboratoire de Thermodynamique Chimique et Appliquée, Ecole Nationale Supérieure des Industries Chimiques, Institut National Polytechnique de Lorraine, 1, rue Grandville-BP 451, 54001 Nancy Cédex, France

Received 21 December 1993; accepted 31 May 1994

Abstract

X-ray diffraction patterns of binary mixtures of normal tricosane and tetracosane at 20°C (powder method) show the presence of two new phases, here denoted β' and β'_1. The crystal structure of these phases is orthorhombic; the structure of the β' phase is isomorphous with the tricosane β' phase observed after the δ transition. With increasing temperature and concentration, the experimental observations, both by X-ray diffraction and differential thermal analysis, made it possible to modify the binary phase diagram of n-C_{23}–n-C_{24}.

Keywords: Binary system; DTA; Tetracosane; Tricosane; XRD

1. Introduction

An estimate of the crystallization point of fuels is possible only when the thermodynamic properties of the pure components and their respective mixtures are known. Moreover, the thermodynamic properties of normal paraffins are closely related to their structural properties. This has prompted a number of crystallographic studies with the aim of determining the relationships between properties and structures.

In our laboratory we are currently undertaking joint thermodynamic and structural studies on the liquid/solid equilibria and transformations in the solid state

* Corresponding author.

SSDI 0040-6031(94)01923-5

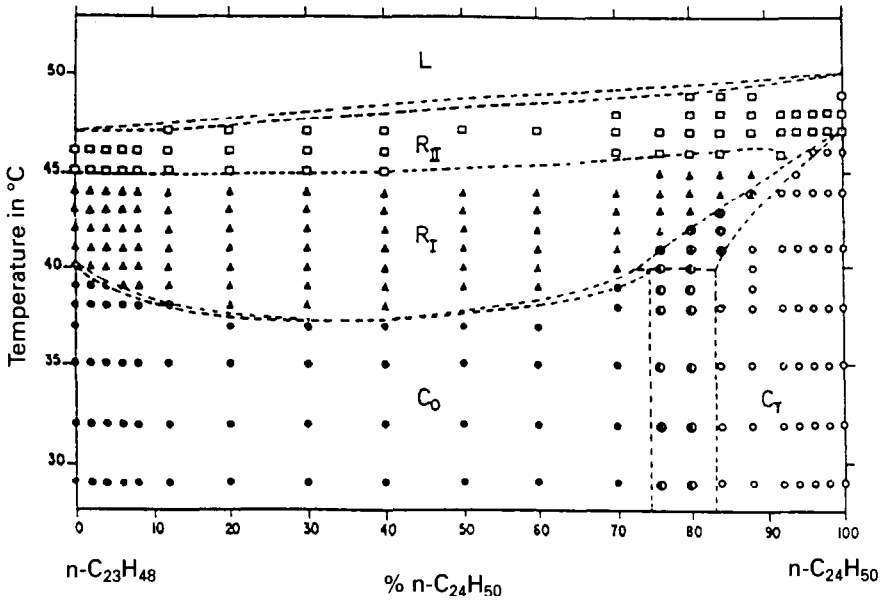

Fig. 1. Phase diagram of n-$C_{23}H_{48}$–n-$C_{23}H_{50}$ mixtures as suggested by Denicolo et al. [11].

occurring in the pure n-alkanes found in fuels [1–3] and in their mixtures [4–8] for which Mazee [9] and Turner [10] have proposed phase diagrams. This work deals with the structural behaviour of tricosane n-C_{23}–tetracosane n-C_{24} mixtures as a function of molar concentration, up to a concentration of 75% n-C_{24}.

Denicolo et al. [11] suggested a phase diagram (Fig. 1) which provides the following information.

(1) The orthorhombic terminal solid solution C_0 shows a homogeneity range up to 75 mol% of tetracosane n-C_{24} at low temperature. Its structure is that of the β_0 tricosane n-C_{23}.

(2) Only two transformations take place in the solid state of tricosane n-C_{23} when the temperature is increased: $C_0 \rightarrow RI \rightarrow \alpha RII$.

However, Ungar and Masic [12] found four transitions: $\beta_0(C_0) \rightarrow \beta' \rightarrow \beta \rightarrow RI \rightarrow \alpha RII$, and these results were later confirmed by Hasnaoui et al. [5].

These contradictory results suggest that the n-C_{23}–n-C_{24} phase diagram is more complex than the diagram shown in Fig. 1.

2. Experimental methods

The mixtures were obtained by melting appropriate proportions of tricosane and tetracosane. The two n-paraffins were supplied by the Aldrich company; their purity grade was analysed by gas chromatography and was found to be 99% for tetracosane and >99% for tricosane.

X-ray diffraction experiments were carried out on powder samples using the Cu Kα radiation.

The X-ray patterns were made with a Guinier de Wolff Nonius chamber, which allows both a clear separation of the wide-angle Bragg reflections and observation of the structural behaviour with concentration. The exposure time was 24 h, using an X-beam obtained with a 10 mA filament, at 50 kV voltage, using a copper anti-cathode. The spacings on the X-ray patterns were measured with an accuracy of 0.25 mm.

The X-ray diffractograms obtained by means of a C.G.R. goniometer are more sensitive at small angles, thus allowing more accurate analysis of the long axis in the c direction of the molecular chain. The calibration was obtained using the (1 1 1) and (2 0 0) Bragg reflections of the face-centred cubic structure of pure aluminium, of which the sample holder was made. The Bragg angles were measured with an accuracy of 1/20th of a degree.

The sample holder was equipped with a heating cell and the samples were held at constant temperature (± 0.05°C) during the X-ray diffraction measurements.

The differential thermal analysis (DTA) experiments were performed using a Setaram DSC 111G calorimeter.

We used both X-ray diffraction and DTA to determine the solid transition temperatures.

3. Structures of tricosane and tetracosane

Keller [13], Broadhurst [14], and Heyding et al. [15] have described the differences between the orthorhombic and triclinic structures of odd-numbered and even-numbered n-alkanes respectively. Nyburg and coworkers [16–19] have identified the structures of even-numbered n-paraffins ($n = 10$, 12, 14, 16, 18) and allotted them the triclinic space group $P\bar{1}$.

At 20°C, n-C_{23} tricosane and n-C_{24} tetracosane respectively exhibit orthorhombic (Pbcm) and triclinic ($P\bar{1}$) structures, denoted β_0 and γ which seem to correspond to the terminal solid solutions C_0 and C_T in the diagram given in Fig. 1.

The lattice spacings determined both experimentally and by calculation, as well as the intensities of the Bragg reflections obtained from the X-ray patterns (Fig. 2) and from the diffractograms (Figs. 3 and 4) performed at room temperature (20°C), are listed in Table 1.

Table 2 compares the experimentally determined crystalline parameters of β_0 n-C_{23} and γ n-C_{24}, with those that were extrapolated to 20°C on the basis of the values published by Denicolo et al. [20].

With increasing temperature, solid phase transitions occur in the n-C_{23} tricosane and n-C_{24} tetracosane.

(1) The triclinic phase γ (n-C_{24}) undergoes a transformation which gives the rhombohedral structure α-RII ($R\bar{3}m$), also seen in even-numbered alkanes with $n = 2p$ ($p > 10$ (11, 20, 21)).

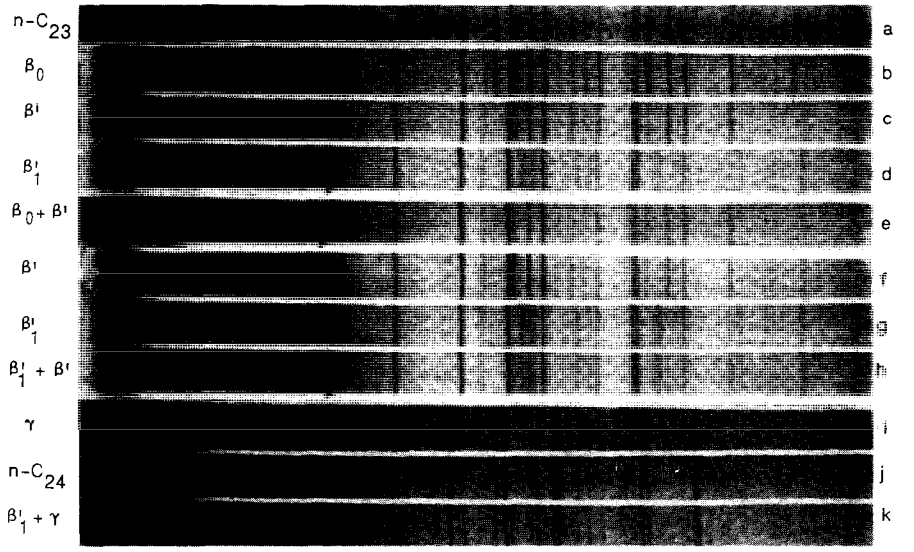

Fig. 2. X-ray diffraction patterns made with a Guinier de Wolff Nonius chamber for n-C_{23}–n-C_{24} mixtures: a, n-C_{23}; b, 0.5% n-C_{24}; c, 2.5% n-C_{24}; d, 10% n-C_{24}; e, 1.5% n-C_{24}; f, 2% n-C_{24}; g, 5% n-C_{24} h, 4% n-C_{24}; i, 90% n-C_{24}; j, n-C_{24}; k, 80% n-C_{24}.

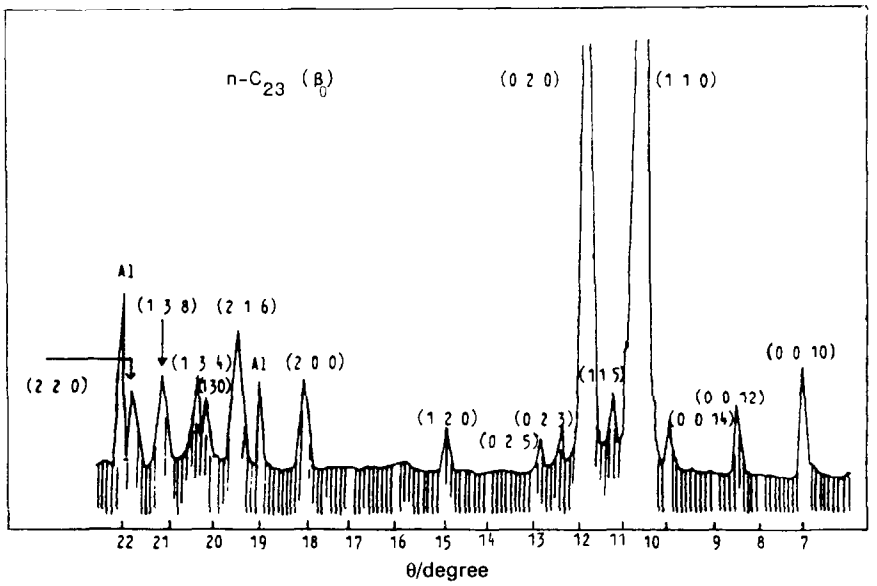

Fig. 3. X-ray diffractogram of tricosane n-C_{23} at 20°C (Cu Kα).

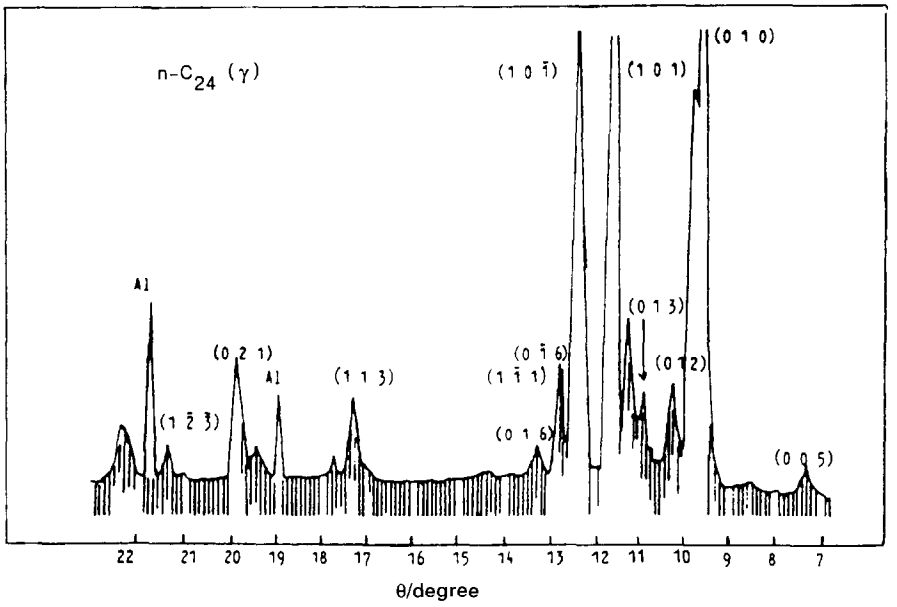

Fig. 4. X-ray diffractogram of tetracosane n-C_{24} at 20°C (Cu Kα).

(2) Doucet et al. [21], Ungar and Masic [12,22], Snyder and Maroncelli [23] and Hasnaoui et al. [5] characterized the solid phase transitions in the n-C_{23} tricosane by X-ray diffraction and DTA

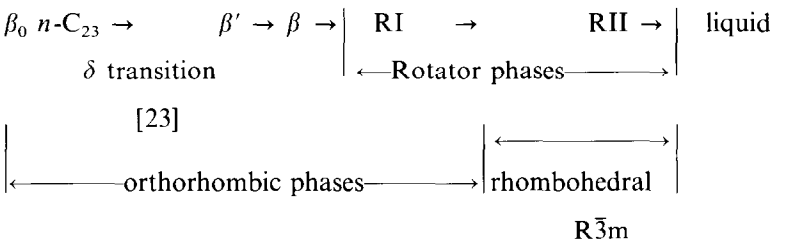

4. Structural behaviour versus tetracosane concentration at room temperature, 20°C

Variations in the Bragg diffractions can be noted on the X-ray patterns (Fig. 2, patterns b,c,d), depending on n-C_{24} concentrations for molar concentrations of 0.5%, 25% and 10% n-C_{24}, respectively.

The lattice spacings and the intensities as recorded experimentally are listed in Table 3. From these values we can conclude that the structure of these phases, denoted β' 2.5% and β'_1 10%, are orthorhombic; the parameters are listed in Table 4.

Table 1
Lattice spacing determined both experimentally from the X-ray patterns and by calculation

Tricosane				Tetracosane			
$a = 0.4958$ nm	$b = 0.7447$ nm	$c = 6.2154$ nm		$a = 0.411$ nm	$b = 0.7447$ nm	$c = 6.2154$ nm	
$\alpha = 90°$	$\beta = 90°$	$\gamma = 90°$		$\alpha = 97.24°$	$\beta = 72.82°$	$\gamma = 107.76°$	
$h\,k\,l$	d_{exp}/nm	d_{cal}/nm	I_{obs}	$h\,k\,l$	d_{exp}/nm	d_{cal}/nm	I_{obs}
0 0 6	1.0398	1.0401	M	0 0 1	3.0648		M
0 0 8	0.7688	0.7788	M	0 0 2	1.5223	1.521	M
0 0 10	0.6145	0.619	M	0 0 3	1.0108	1.014	M
0 0 12	0.5180	0.5185	M	0 0 4	0.7621	0.760	M
0 0 14	0.4431	0.4438	W	0 0 5	0.6061	0.608	M
1 1 0	0.412	0.4139	VS	0 1 0	0.4571	0.4568	S
1 1 3	0.4036	0.4059	S	0 1 1	0.4497	0.4495	S
1 1 5	0.388	0.3928	S	0 1 2	0.4345	0.434	M
0 2 0	0.3704	0.3739	VS	0 1 3	0.411	0.412	M
0 2 3	0.3630	0.3679	M	1 0 1	0.3814	0.3812	S
0 2 5	0.353	0.3581	M	1 0 $\bar{1}$	0.3572	0.3577	S
1 1 10	0.341	0.344	W	0 1 6	0.3503	0.3508	M
1 1 11	0.332	0.3341	W	1 1 1	0.3476	0.3474	M
1 2 0	0.2961	0.2987	S	0 1 6	0.337	0.3373	W
2 0 0	0.2462	0.2485	S	1 1 3	0.2578	0.2578	M
2 0 7	–	0.2393	–	0 2 1	0.2270	0.2271	M
2 1 0	0.2330	0.2358	M	1 2 3	0.2112	0.2113	W
2 1 6	0.2279	0.2279	M	2 1 7	0.1596	0.1595	M
1 3 0	0.2209	0.2228	S				
1 3 4	0.218	0.2205	M				
1 3 8	0.2120	0.2142	M				
2 2 0	0.2056	0.2069	S				
2 2 8	0.2012	0.20	W				
2 2 9	–	0.198	–				
2 2 10	0.1941	0.1951	W				
2 2 11	–	0.1927	–				
2 2 12	0.191	0.1910	W				
2 2 13	–	0.1884	–				
0 4 2	0.1857	0.1866	M				
0 4 11	0.1764	0.1768	M				
2 3 0	0.1743	0.1759	M				
2 3 5	0.1732	0.1742	M				
1 4 7	0.1699	0.1716	S				
3 0 2	0.1646	0.1654	S				
3 1 2	0.1603	0.1615	S				
3 2 3	0.1502	0.1510	S				
1 5 10	0.1398	0.1410	S				

The lattice parameters were determined with a relative error of 0.3%. Key: W, weak; M, medium; S, strong; VS, very strong.

Table 2
Lattice parameters of tricosane and tetracosane at 20°C

Parameters	β_0 n-$C_{23}H_{48}$		γ n-$C_{24}H_{50}$	
	Denicolo et al. [20]	This work	Denicolo et al. [20]	This work
a/nm	0.497	0.496 ± 0.0015	0.405	0.411 ± 0.0015
b/nm	0.7478	0.745 ± 0.002	0.4801	0.480 ± 0.0015
c/nm	6.2310	6.215 ± 0.02	3.284	3.20 ± 0.02
α/°	90	90	97.24	97.24
β/°	90	90	72.82	72.82
γ/°	90	90	107.76	107.76.

It is interesting to compare the results of the X-ray diffraction measurements, Table 3, as regards the structures of these β' and β'_1 phases, with the results obtained with a powder sample of the terminal solid solution β_0 n-C_{23}.

5. A comparison of the X-ray patterns of the β' phase and of the β_0 and β' n-C_{23} phases

5.1. Variations on the X-ray patterns from the terminal solid solution β_0 n-C_{23} *to phase* β'

The behaviour of the low-temperature orthorhombic structure of tricosane, β_0 with Pbcm space group [24], as observed in the mixture with 1.5% n-C_{24} molar concentration, varies as shown in Fig. 2, patterns a,c,e, and Table 3: lines (2 1 6) and (1 5 10) disappear; line (2 0 7) appears; the intensities of the Bragg diffractions (1 3 0) and (2 3 5) increase; and the intensities of the lines (0 4 11) and (1 4 7) decrease.

5.2. Similarity of β' *and* β' n-C_{23} *phases*

The above modifications are similar to those recorded by Ungar and Masic [12,22] and Hasnaoui et al. [5] in their studies on the structural behaviour of n-C_{23} tricosane as a function of temperature. They also correspond, in this particular case, to the δ transition ($\beta_0 \rightarrow \beta'$), also observed by Snyder [23]. This observation allows us to state that the β' n-C_{23} phase and the β' phase are identical. The β' phase in this mixture is actually the solid terminal solution of n-C_{24} in the high-temperature β' n-C_{23} phase. An increase in the disorder of the crystallographic structure of tricosane is produced by the presence of a few percent of tetracosane which can therefore be said to have the same effect as temperature.

Table 3
Lattice spacing determined both experimentally and calculated, (h k l) index of reflection phases, and intensities estimated for β_0 (0.5%), β' (2.5%) and β'_1 (10%) phases in n-C_{24}

h k l	Phase β_0, tricosane			Phase β_0 (0.5%)			Phase β' (2.5%)			Phase β'_1 (10%)		
	d/nm (exp.)	*d*/nm (calc.)	*I*	*d*/nm (exp.)	*d*/nm (calc.)	*I*	*d*/nm (exp.)	*d*/nm (calc.)	*I*	*d*/nm (exp.)	*d*/nm (calc.)	*I*
0 0 6	1.0398	1.0401	M	1.0393	1.0359	M	1.0393	1.0434	M	1.0455	1.0498	M
0 0 8	0.7688	0.7788	M	0.7755	0.7769	M	0.7858	0.7825	M	0.7893	0.7873	M
0 0 10	0.6145	0.619	M	0.6210	0.6210	M	0.6254	0.6260	M	0.6314	0.6299	M
0 0 12	0.5180	0.5185	M	0.5179	0.5179	M	0.5241	0.5217	M	0.5249	0.5249	M
0 0 14	0.4431	0.4438	W	0.4435	0.4439	W	0.4446	0.4471	W	0.4491	0.4499	W
1 1 0	0.412	0.4139	VS	0.4129	0.4127	VS	0.4129	0.4127	VS	0.4129	0.4127	VS
1 1 3	0.4036	0.4059	S	0.4036	0.4047	S	0.4036	0.4049	S	0.4036	0.4049	S
1 1 5	0.388	0.3928	S	0.3913	0.3917	S	0.3922	0.3919	S	0.3922	0.3922	S
0 2 0	0.3704	0.3739	VS	0.3723	0.3723	VS	0.3723	0.3723	VS	0.3723	0.3723	VS
0 2 3	0.3630	0.3679	M	0.3667	0.3665	M	0.3667	0.3665	M	0.3667	0.3666	M
0 2 5	0.3530	0.3581	M	0.3558	0.3567	M	0.3558	0.3569	M	0.3551	0.3571	M
1 1 10	0.341	0.3440	W	0.3438	0.3438	W	0.3440	0.3445	W	0.3424	0.3452	W
1 1 11	0.3320	0.3341	W	0.3329	0.3332	W	0.3335	0.3341	W	0.3329	0.3348	W
1 2 0	0.2961	0.2987	S	0.2976	0.2977	S	0.2976	0.2977	S	0.2976	0.2977	S
2 0 0	0.2462	0.2485	S	0.2479	0.2479	S	0.2479	0.2479	S	0.2479	0.2479	S
2 0 7 △	–	0.2393	–	–	0.2387	–	0.2380	0.2389	W	0.2380	0.2390	W
2 1 0	0.2330	0.2358	M	0.2353	0.2352	M	0.2353	0.2352	M	0.2353	0.2352	M
2 1 6 △	0.2279	0.2279	M	0.2293	0.2293	M	–	0.2294	–	–	0.2295	–
1 3 0 △	0.2209	0.2228	S	0.2219	0.2219	S	0.2218	0.2219	VS	0.2218	0.2219	VS
1 3 4 *	0.218	0.2205	M	0.2192	0.2197	M	0.2193	0.2197	M	–	0.2198	–
1 3 8 *	0.2120	0.2142	M	0.2125	0.2134	M	0.2125	0.2135	M	0.2125	0.2136	↔
2 2 0	0.2056	0.2069	S	0.2063	0.2063	S	0.2067	0.2063	S	0.2067	0.2063	S
2 2 8 *	0.2012	0.200	S	0.2008	0.1994	W	0.2008	0.1995	W	–	0.1996	–
2 2 9 *	–	0.198	–	–	0.1977	–	–	0.1978	–	0.1981	0.1979	W
2 2 10 *	0.1941	0.1951	W	0.1955	0.1958	W	0.1951	0.1959	W	–	0.1961	–
2 2 11 *	–	0.1927	–	–	0.1938	–	–	0.1940	–	0.1931	0.1941	M

2 2 12	*	0.191	0.1910	–	0.1908	0.1917	W	0.1908	0.1919	W	–	0.1920	–
2 2 13	*	–	0.1884	–	–	0.1894	–	–	0.1896	–	0.1889	0.1898	M
0 4 2		0.1857	0.1866	–	0.1857	0.1858	M	0.1857	0.1858	M	0.1860	0.1858	M
0 4 11	△*	0.1764	0.1768	M	0.1771	0.1768	M	0.1772	0.1769	W	–	0.1770	–
2 3 0	*	0.1743	0.1759	M	0.1754	0.1754	M	0.1753	0.1754	M	0.1753	0.1754	S
2 3 5	△	0.1732	0.1742	M	0.1737	0.1737	M	0.1738	0.1737	S	0.1733	0.1737	S
1 4 7	△*	0.1699	0.1716	M	0.1707	0.1701	M	0.1711	0.1710	W	–	0.1711	–
3 0 2	*	0.1646	0.1654	S	0.1650	0.1650	S	0.1654	0.1650	S	–	0.1650	–
3 1 2	*	0.1603	0.1615	S	0.1611	0.1611	S	0.1611	0.1611	S	0.1614	0.1611	M
3 2 3	*	0.1502	0.1510	S	0.1506	0.1506	S	0.1508	0.1506	S	0.1508	0.1506	M
1 5 10	△	0.1398	0.1410	S	0.1390	0.1390	S	–	0.1390	–	–	0.1391	–

Symbols: ↔, the line widens; – the line disappears, △ lines which characterize the ($\beta_0 \rightarrow \beta'$) transition; *, lines which characterize the ($\beta' \rightarrow \beta'_1$) transition.
Key: S, line of strong intensity; M, line of medium intensity; W, line of weak intensity; VS, line of very strong intensity.

Table 4
Variations in the lattice parameters of the mixtures as a function of tetracosane concentration

Parameter	β_0 n-C_{23}	β_0	β'	β'_1
Molar concentration of n-C_{24}	0%	0.5%	2.5%	10%
a/nm	0.496 ± 0.0015	0.496 ± 0.0015	0.496 ± 0.0015	0.496 ± 0.0015
b/nm	0.745 ± 0.002	0.745 ± 0.002	0.4475 ± 0.0015	0.4475 ± 0.0015
c/nm	6.215 ± 0.02	6.215 ± 0.02	6.2365 ± 0.02	6.30 ± 0.02

6. Variations from the β' phase to the intermediate β'_1 phase

The mixture with 10% n-C_{24} molar concentration exhibits the orthorhombic structure of the intermediate β'_1 phase. As compared with the β' phase, this is reflected by the following features (Fig. 2, patterns c,d, and Table 3): lines (1 3 4), (0 4 11), (1 4 7), (3 0 2) and (2 2 l), where $l = 2n$ ($4 < n < 6$), disappear; line (1 3 8) widens; intensities of lines (3 1 2) and (3 2 3) decrease; intensity of line (2 3 0) increases; lines (2 2 l) appear, where $l = 3n + 2k$, $n = 3$ ($0 < k < 2$).

7. Domains of existence of solid solutions as a function of tetracosane concentration at room temperature, 20°C

We have prepared twelve mixtures with increasing n-C_{24} molar concentrations in order to determine the solubility domain of tetracosane in the β_0 and β' structures of tricosane, the domain of existence of the new intermediate β'_1 phase, and the two-phase domains, $\beta_0 + \beta'$, $\beta' + \beta'_1$ at room temperature, 20°C.

In order to estimate the domains of one-phase and two-phase concentration, we use as a criterion the average distance d between the stacking planes of a layer of molecules, this value being obtained from the values of the (0 0 l)-type diffraction lines on the X-ray patterns: in one-phase domains, a linear increase of this value can be noted, depending on the n-C_{24} concentration (Fig. 5); in two-phase domains, the phase ratio alone varies, whereas the crystalline parameters remain constant (Fig. 5).

7.1. *The terminal solid solution* β_0

The X-ray patterns made for the mixtures with n-C_{24} concentration ranging from 0.5% to 1.3% correspond to the β_0 orthorhombic structure of n-C_{23}.

7.2. *The* β' *solid solution*

From the 2% concentration in n-C_{24}, the reflections characteristically belonging to the β_0 structure lines (2 1 6) and (1 5 10) have completely disappeared (Fig. 2,

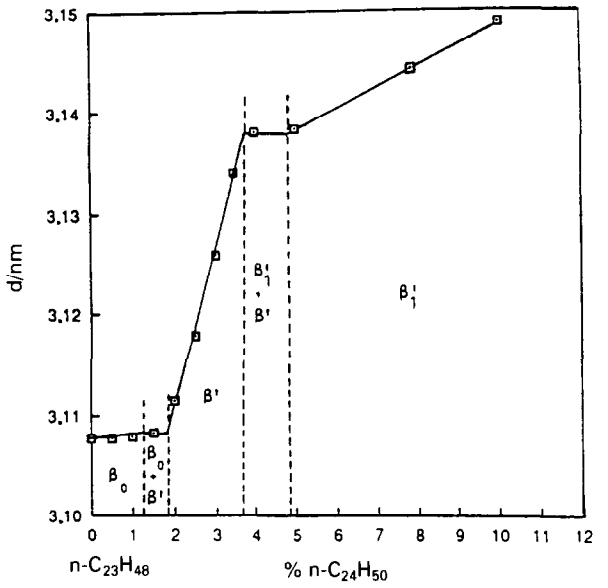

Fig. 5. The lattice spacing d variation between the stacking planes of a layer of molecules, as a function of n-C_{24} molar concentration for solutions rich in n-C_{23} ($d = c/2$).

pattern f). We enter the β' one-phase domain which in tricosane n-C_{23} is observed after the δ transition. This β' domain extends up to the molar concentration of 3.5% in n-C_{24}.

7.3. The β'_1 intermediate solid solution

This β'_1 phase exists in the one-phase state for the molar concentration higher than 5% in n-C_{24}. The reflections belonging to the β' phase have disappeared (Fig. 2, pattern g) and the domain extends up to 75% molar concentration in n-C_{24}.

Both the observation of the X-ray diffraction patterns and the study of the variations of the distance between the stacking planes allow us to determine the domains of existence from 0% to 75% in n-C_{24} at 20°C (Figs. 5 and 6):

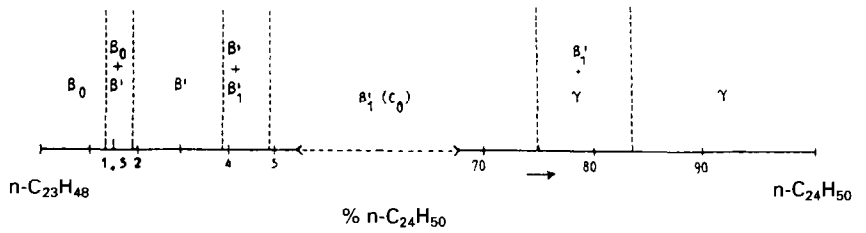

Fig. 6. Domains of existence of phases for binary mixtures of n-C_{23}–n-C_{24} as a function of molar concentration in n-C_{24} at 20°C.

(1) Three one-phase domains: $0 < x < 1.5\%$, orthorhombic terminal solid solution β_0 n-C_{23}; $1.8 < x < 4\%$, β' solid solution, having an orthorhombic structure, isomorphous with the structure of tricosane n-C_{23} observed after the δ transition; $4.8 < x < 75\%$, intermediate solid solution, β'_1 orthorhombic structure.

(2) Two two-phase domains: $1.3 < x < 2\%$, β_0 n-$C_{23} + \beta'$ (Fig. 2, pattern e); $3.5 < x < 5\%$, $\beta' + \beta'_1$ (Fig. 2, pattern h).

Beyond $x = 75\%$, we observe the same results as Denicolo et al. [11].

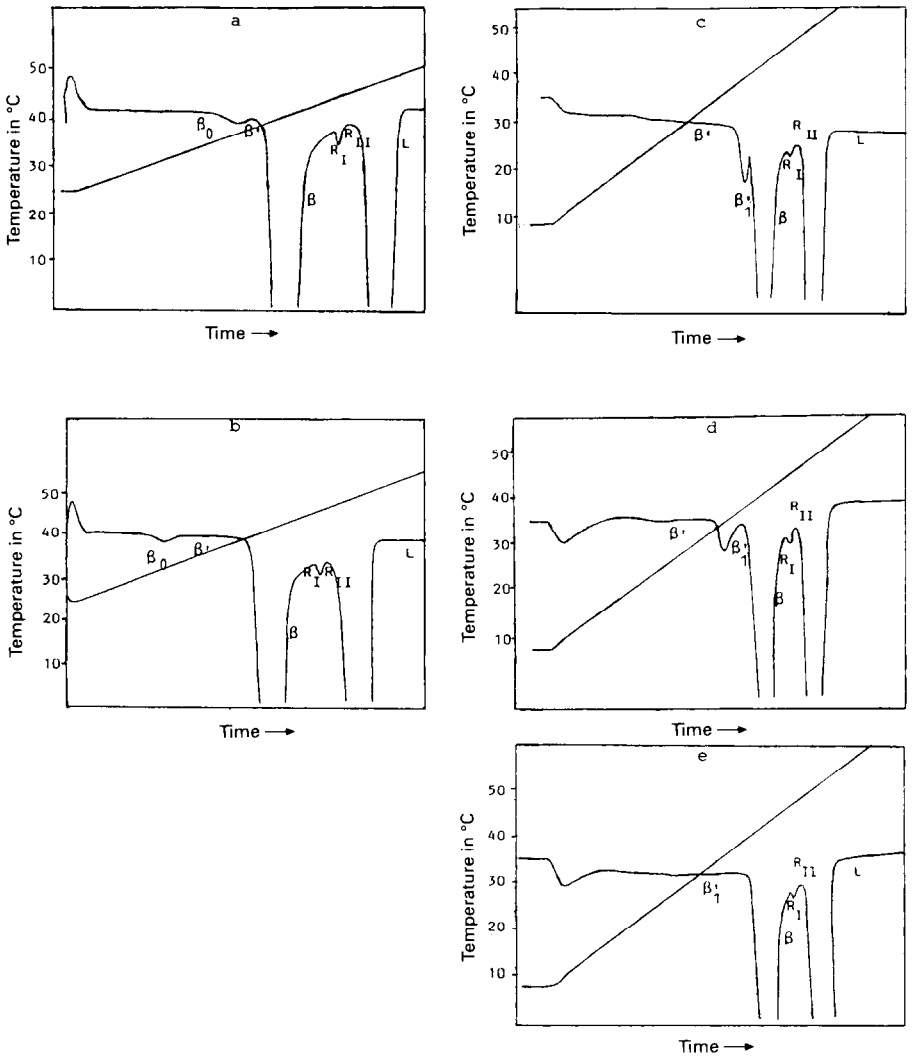

Fig. 7. DTA curves of n-$C_{23}H_{48}$–n-$C_{24}H_{50}$ mixtures. Compositions are given in molar concentration of n-$C_{24}H_{50}$: a, 0.5%; b, 1%; c, 1.5%; d, 2.5%, e, 5%.

8. Structural behaviour with increasing temperature and n-C_{24} molar concentration

The differential thermal analysis was performed on twenty binary mixtures heated at a rate of 0.5°C min^{-1} from 8°C up to above the liquidus. The DTA curves for different concentrations are shown in Fig. 7. The solid phase structures were characterized by X-ray diffraction analyses on samples from either side of DTA peaks.

The sequence of peaks for the first terminal solid solution β_0 n-C_{23} (Fig. 7a,b) is similar to that obtained in pure n-C_{23} tricosane [12,21–23]

β_0 n-C_{23} → β' → β → RI → RII → liquid

δ transition ←—Rotator phases—→

[23]

←—orthorhombic phases—→ ←→ rhombohedral

$R\bar{3}m$

The solid phase succession from low to high temperatures for the second terminal solid solution β' corresponds to the results (Fig. 7c,d)

β' → β'_1 → β → RI → RII → liquid

←—orthorhombic phases—→ rhombohedral

$R\bar{3}m$

The intermediate phase β'_1 undergoes peritectoid decomposition

$\beta'_1 \rightarrow \beta' + \beta$ at 39.3 ± 0.1°C

The simple thermal analysis with decreasing temperature from the liquid state to room temperature shows the existence of this invariant point (Fig. 8).

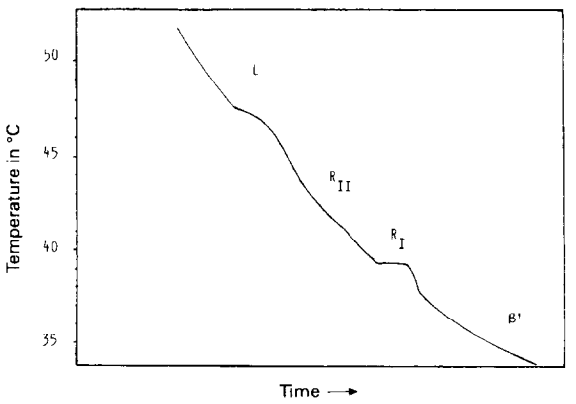

Fig. 8. Simple thermal analysis curve (binary mixture of 1.5% n-$C_{24}H_{50}$).

Above the two-phase domain ($\beta' + \beta$), the orthorhombic solution β appears and transforms into Rotator I (RI), also orthorhombic. Just below the solidus line, the rhomboedral (α-RII) phase exists.

9. Conclusion — the phase diagram

The above structural study of n-C_{23}–n-C_{24} binary mixtures allows us to establish the existence at 293.2 K of two new phases, denoted β' and β'_1, both having an

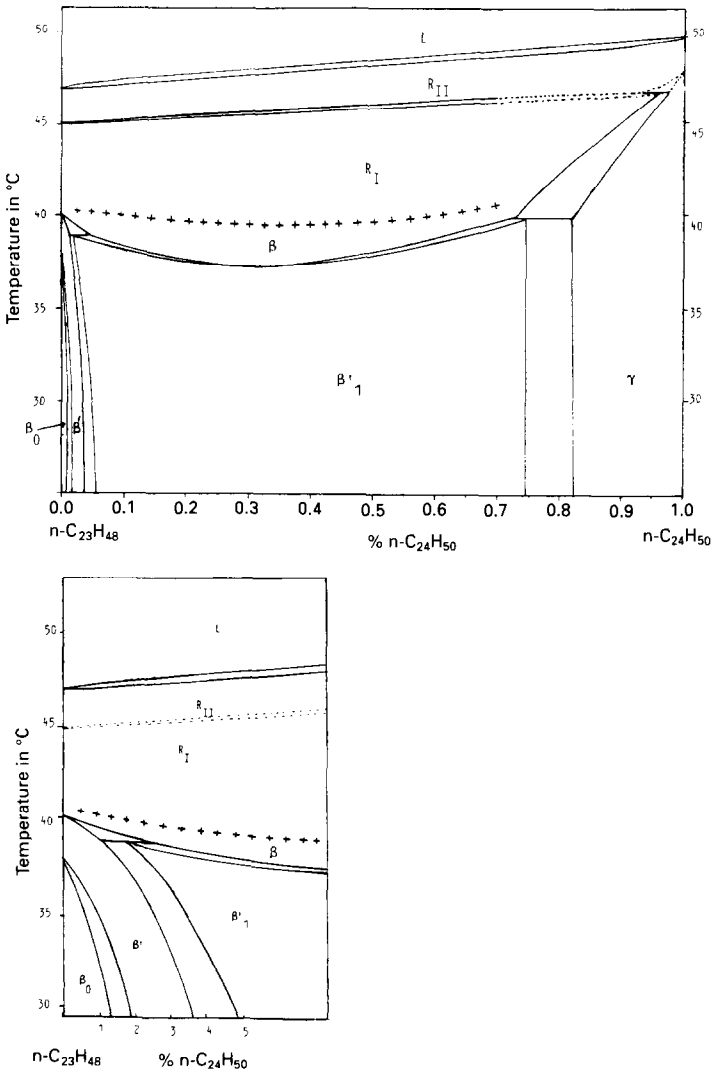

Fig. 9. Phase diagram of n-$C_{23}H_{48}$–n-$C_{24}H_{50}$ mixtures as suggested by our work.

orthorhombic structure. The first of these two phases corresponds to the β' phase of tricosane which appears in the pure compound after the δ transition [23]. The second corresponds to an intermediate solid solution.

With increasing temperature, the experimental observations, together with the X-ray diffraction and differential thermal analysis results, show the existence of four solid transitions for the two terminal solid solutions β_0 and β' n-C_{23}; and three solid transitions for the intermediate solid solution β'_1, the first of these being a peritectoid decomposition.

These new results made it possible to modify the binary phase diagram of n-C_{23}–n-C_{24} over the concentration range from 0 to 75 mol% n-C_{24} (Fig. 9). Beyond $x = 75\%$, we observe the same results as Denicolo et al. [11] except, however, for C_0 which is replaced by β'_1, and the triclinic terminal solid solution C_T (n-C_{24}) which is replaced by γ.

References

[1] P. Barbillon, L. Schuffenecker, J. Dellacherie, D. Balesdent and M. Dirand, J. Chim. Phys., 88 (1991) 91.
[2] P.M. Ghoghomu, J. Dellacherie and D. Balesdent, J. Chem. Thermodyn., 21 (1989) 925.
[3] P.M. Ghogomu, J. Dellacherie and D. Balesdent, Thermochim. Acta, 157 (1990) 241.
[4] N. Hasnaoui, J. Dellacherie, L. Schuffenecker, M. Dirand and D. Balesdent, J. Chim. Phys., 85(2) (1988) 153.
[5] N. Hasnaoui, J. Dellacherie, L. Schuffenecker, M. Dirand and D. Balesdent, J. Chim. Phys., 85(6) (1988) 675.
[6] Z. Achour, J.B. Bourdet, M. Bouroukba and M. Dirand, J. Chim. Phys., 89 (1992) 707.
[7] Z. Achour, J.B. Bourdet, M. Bouroukba and M. Dirand, Thermochim. Acta, 204 (1992) 187.
[8] Z. Achour, J.B. Bourdet, M. Bouroukba and M. Dirand, J. Chim. Phys., 90 (1993) 325.
[9] W.M. Mazee, Am. Chem. Soc., Meeting Symp. Div. Pet. Chem., Chicago, (1958).
[10] W.R. Turner, Ind. Eng. Chem. Prod. Res., Dev., 10(3) (1971) 238.
[11] I. Denicolo, A.F. Craievich and J. Doucet, J. Chem. Phys., 80(12) (1984) 6200.
[12] G. Ungar and G. Masic, J. Phys. Chem., 89 (1985) 1036.
[13] A. Keller, Philos. Mag., 6(63) (1961) 329.
[14] M.J. Broadhurst, J. Res. Natl. Bur. Stand. Sect. A, 66 (1962) 241.
[15] R.D. Heyding, K.E. Russel, T.L. Varty and D. St Cyr, Powder Diffraction, 5(2) (1990) 93.
[16] S.C. Nyburg and H. Luth, Acta Crystallogr. Sect. B, 28 (1972) 2992.
[17] S.C. Nyburg and J.A. Potworowski, Acta Crystallogr. Sect. B, 29 (1973) 347.
[18] S.C. Nyburg and F.M. Pickard, Acta Crystallogr. Sect. B, 30 (1974) 1885.
[19] S.C. Nyburg and F.M. Pickard, Acta Crystallogr. Sect. B, 32 (1976) 2289.
[20] I. Denicolo, J. Doucet and A.F. Craievich, J. Chem. Phys., 78 (1983) 1465.
[21] J. Doucet, I. Denicolo, A.F. Crewich and C. Germain, J. Chem. Phys., 80(4) (1984) 1647.
[22] G. Ungar, J. Phys. Chem., 87 (1983) 689.
[23] R.G. Snyder and M. Maroncelli, Science, 214 (1981) 188.
[24] A.E. Smith, J. Chem. Phys., 21 (1953) 2229.